Molecular Crystals and Liquid Crystals

ISSN: 1542-1406 (Print) 1563-5287 (Online) Journal homepage: http://www.tandfonline.com/loi/gmcl20

Flow-induced Alignment of Disk-like Graphene Oxide Particles in Isotropic and Biphasic Colloids

Seung-Ho Hong, Tian-Zi Shen & Jang-Kun Song

To cite this article: Seung-Ho Hong, Tian-Zi Shen & Jang-Kun Song (2015) Flow-induced Alignment of Disk-like Graphene Oxide Particles in Isotropic and Biphasic Colloids, Molecular Crystals and Liquid Crystals, 610:1, 68-76, DOI: 10.1080/15421406.2015.1025208

To link to this article: http://dx.doi.org/10.1080/15421406.2015.1025208

Published online: 06 Jul 2015.

Mol. Cryst. Liq. Cryst., Vol. 610: pp. 68–76, 2015

ISSN: 1542-1406 print/1563-5287 online
DOI: 10.1080/15421406.2015.1025208

Flow-induced Alignment of Disk-like Graphene Oxide Particles in Isotropic and Biphasic Colloids

SEUNG-HO HONG, TIAN-ZI SHEN, AND JANG-KUN SONG*

School of Electronic & Electrical Engineering, Sungkyunkwan University, Suwon, Republic of Korea

The flow-induced ordering of Graphene oxide (GO) particles was investigated in a tube flow of aqueous GO dispersions with varying GO concentrations. By measuring the average effective birefringence for the samples in a tube flow, we could quantitatively deduce the order parameter of GO particles. The flow-induced effective birefringence linearly increased as the GO concentration increased in isotropic phase, but the birefringence deviated from the linear tendency and increased more in biphase. We also calculated the S *and* P *order parameters using the optical birefringence profile in the tube flow. The result showed that the* S *order parameter kept increasing as the GO concentration increased but the* P *order parameter decreased as the GO concentration increased. All these results indicate that the increase in inter-particle ordering interaction in biphase enhances the uniaxial* S *order parameter in the flow-induced ordering and suppresses the biased biaxial ordering.*

Keywords Graphene oxide, flow-induced ordering, liquid crystal, colloid

Introduction

Graphene oxide (GO) has unique mechanical, thermal and optical properties that can be useful in many corresponding applications [1,2,3]. Usually, GO is obtained as flakes in aqueous colloid. A GO particle in aqueous colloidal dispersion has very thin thickness about 1 nm and wide diameter up to dozens micrometer, hence a GO particle is regarded as 2-dimentional (2D) material. Aspect ratio of GO particles, that is the ratio between the diameter and the thickness, ranges from 10^2 to 10^4 [4,5]. Onsager's excluded volume theory predicts that 2D material with high aspect ratio can easily form self-aligned nematic phase in relatively low concentrations. Hence, an aqueous GO dispersion exhibits a lyotropic liquid crystal phase in very low concentration less than 1 vol%. The self-aligned liquid crystalline property is also an interesting feature of GO material that can be used in optical application and fabrication of films and fibre [6,7,8].

From rheological point of view, 2 dimensional shape of GO particles can give rise to close correlation between viscosity of GO dispersions and the degree of GO particle ordering, so strong shear thinning phenomenon is commonly observed. Additionally, as we recently reported, the ordering of GO particles can be induced in isotropic phase by

*Address correspondence to Jang-Kun Song, School of Electronic & Electrical Engineering, Sungkyunkwan University, Suwon, Gyeonggi-do, 440-746, Republic of Korea. E-mail: jk.song@skku.edu

Color versions of one or more of the figures in the article can be found online at www.tandfonline.com/gmcl.

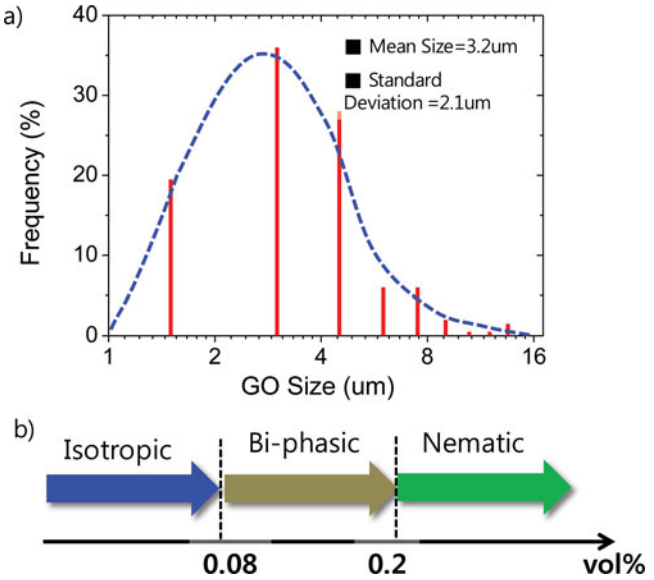

Figure 1. a) The size distribution of GO particles. b) The calculated concentration where the phase transition occurs.

applying electric field or making a flow. In isotropic phase, the inter-particle interaction is too weak to cause the self-aligned nematic phase [9]. The flow-induced alignment of GO particles and the resulting change in rheological aspect is an interesting topic that can be used in microfluidics.

In this paper, we investigated the flow-induced birefringence of GO dispersions as a function of GO concentration in a steady tube flow with a constant mean shear rate. By analysing the optical data, we calculated the S and P order parameters that are associated with the uniaxiality and biaxiality of GO orderings. We found that the flow-induced S order parameter in the biphasic phase was higher than that in the isotropic phase. It implies that the flow induced ordering is closely related to the spontaneous nematic ordering of GO particles.

Sample Preparation

An aqueous GO dispersion was prepared by typical Hummers method [10]. The radius of GO was measured by using scanning electron microscopic (SEM) images. Figure 1(a) shows the distribution of GO size; the mean size was 3.2 μm and the standard deviation was 2.1 μm. The thickness of GO particle, which was measured by atomic force microscopy, was approximately 1nm. Therefore, the aspect ratio was 3200. We can calculate the phase transition concentrations for polydispersed dispersions using the mean size and standard deviation, and their thickness.

According to the calculation, the transition from isotropic to biphase appears at 0.08 vol%, and the transition to nematic phase appears at 0.2 vol%, as shown in Fig. 1(b) [11].

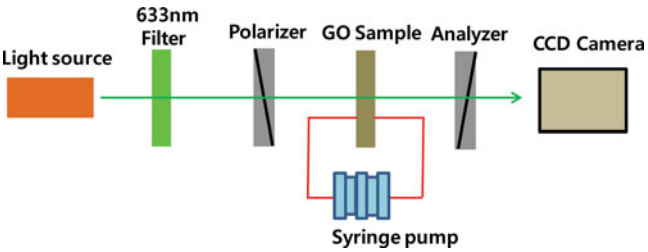

Figure 2. The optical experimental set up for measuring transmittance profile and birefringence.

Experiment

Experimental set-up for the optical measurement is illustrated in Fig. 2. Collimated beam from a halogen lamp passed through a 633nm band pass filter, a polarizer, a GO sample, and an anlayzer, one by one. The angle between the analyzer and the polarizer made 90 degrees. The CCD camera captured the image, which can be analyzed to obtain light intensity profile as a function of position. To produce a steady flow within a circular tube, a syringe pump (Pump 11 Elite, Harvard Apparatus Company) was used. The coordinate systems for the experiments are shown in Fig. 3(a). The circular tube fits with the cylindrical coordinate system; beam path is parallel to Y axis, z-axis is the same as the flow direction, φ-axis and r-axis are the radial and azimuthal axes, respectively. **a** vector is the unit vector normal to the GO basal plane. In this system, the radial direction coincides with the velocity gradient direction of the tube flow and φ-axis is parallel to the vorticity direction of the flow. The measured optical transmittance was used to calculate the optical retardation (R_{eff}) of the cell.

$$\frac{I}{I_0} = \sin^2\left(\frac{\pi \langle \Delta n_{\text{eff}} \rangle l}{\lambda}\right) \equiv \sin^2\left(\frac{\pi R_{\text{eff}}}{\lambda}\right) \tag{1}$$

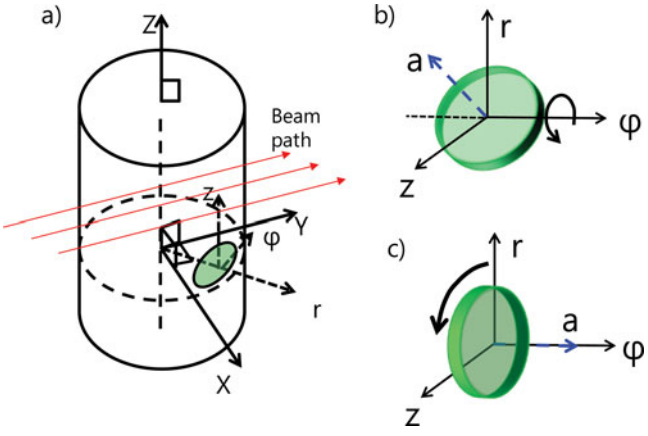

Figure 3. a) The coordinate system used in our system. Beam path is parallel to Y axis. b) Two dominant particle motions are expected theoretically; **a** vector is rotating around the φ axis (designated as mode 1) and c) a GO particle rotates with the rotation axis of **a** vector (mode 2).

Here, I, I_0, and λ are the transmitted light-intensity with steady flow under two crossed polarizers, the intensity with no flow under two parallel polarizers, and the wavelength of the incident light (633 nm).

The effective retardation R_{eff} as a function of the position in the tube was obtained by the multiplication of the average of effective birefringence $<\Delta n_{\text{eff}}>$ and the beam path length l. Here, $<\Delta n_{\text{eff}}>$ is defined as

$$<n_{\text{eff}}>=\frac{1}{l}\int_{l}[n_{\text{Z}}(r)-n_{\text{X}}(r,\varphi)]\text{d}l. \tag{2}$$

The anisotropic colloid in flowing solution has been systematically investigated and it was explicitly confirmed that two typical motions for disk-like particles are expected as shown in the illustration of Fig. 3 (b) and (c), which are designated as mode 1 and 2 [12,13]. For mode 1, the probability density function (Q) of **a** vector as a function of θ, which is the angle between **a** and r-axis, was calculated by Jefferey [14] as

$$Q=\frac{A}{2\pi(\cos^2\theta+A^2\sin^2\theta)}. \tag{3}$$

Here, A is the aspect ratio of GO particles. When A is sufficiently large, Q approaches to the delta function and all GO particles are likely to align to have $\theta=0$, that is, the direction of **a** vector coincides with the z-axis. Generally, as the interaction between two particles increases, the portion of mode 2 increases [12,13]. Optically, mode 1 is related to the birefringence Δn_{zr} between z and r axis and mode 2 produced the birefringence $\Delta n_{z\phi}$ between z and φ axis. Hence, mode 1 is mainly observed in the edge of tube, and mode 2 is mainly observed in the center of tube. There optical birefringence values are measureable using the experimental set-up in Fig. 2.

Flow-Induced Birefringence

The initial state was dark as shown in Fig. 4(a), since the GO dispersions are mostly isotropic. However, the 0.1 vol% GO dispersion showed weak light leakage. 0.1 vol% dispersion is biphase and the injection of GO dispersion into the tube made some flow-induced alignment, which did not disappeared. The initial birefringence for 0.1 vol% is relatively weak compared to the flow-induced birefringence, and the flow-induced birefringence measurement was valid even for 0.1 vol% dispersion. As the flow increased, the optical transmittance increased as well. This is because the flow-induced particle ordering gives rise to optical birefringence. The mean flow velocity for optical measurements was 8.0 mm/sec. The direction of GO particle alignment was parallel to the tube flow, which was optically confirmed by rotating the polarizer and analyzer. When the axis of one of two polarizers is parallel to the tube flow, it looked the darkest, as indicated in Fig. 4(a). The transmittance profile was recorded by CCD camera, and was shown in Fig. 4 (b), in which the half of the transmittance profile was used for convenience. Figure 4(b) showed that the sample with higher concentration has higher optical birefringence. Interestingly, some optical birefringence was detected even at the center of tube, which indicates that non-negligible quantity of particle motions belonging to mode 2 exists in the tube flow. Note that the motion of mode 1 is uniaxial with the radial axis and it cannot produce any birefringence at the center of the tube. To further investigate the flow-induced particle

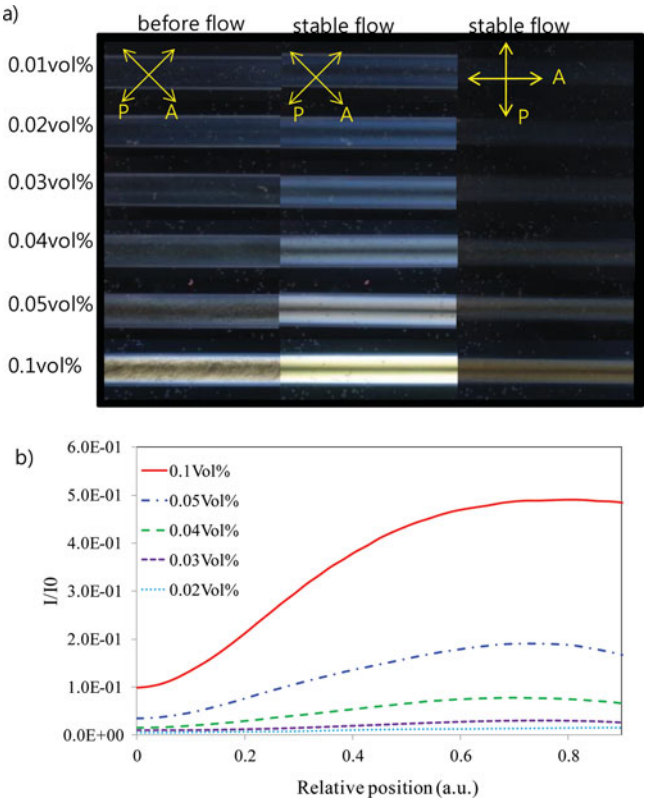

Figure 4. a) Photos of the flow-induced birefringence depending on the concentration. In the first row corresponding to "before flow," the polarizer (P) and the analyzer (A) axis have 45 degree to the flow direction. The second row showed the state of stable flowing, and in the third row, P and A were rotated to 45 degree during the stable flow. b) The transmittance profile in which x-axis was normalized the edge setting the center as zero.

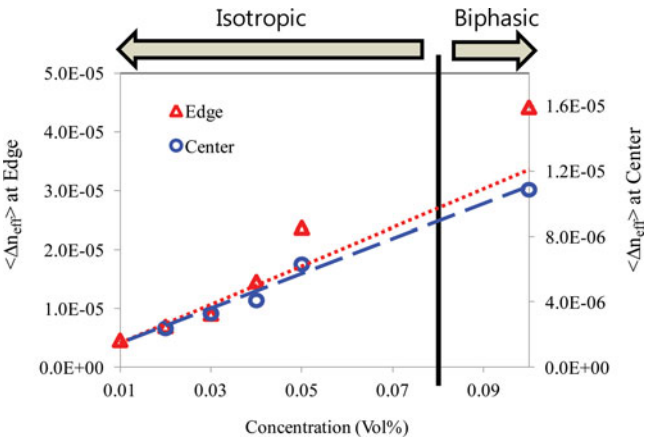

Figure 5. Average effective birefringence at the edge (triangle) and at the center (circle) depending on the concentration.

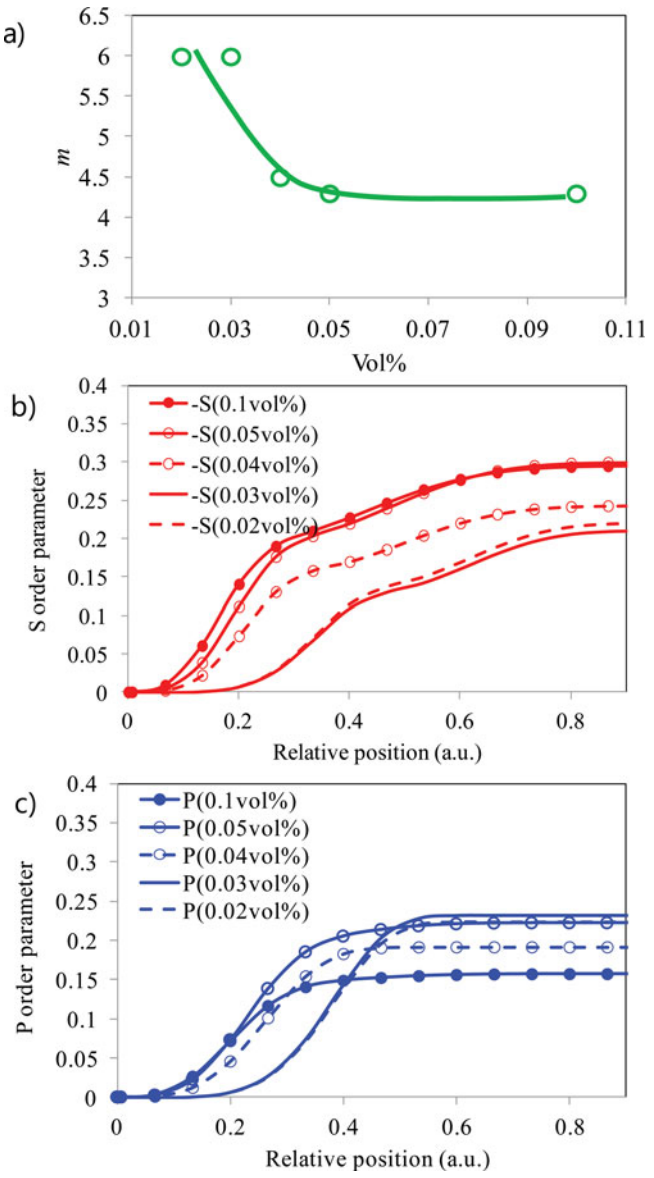

Figure 6. a) Simulated *m* for the best fit depending on the concentration. b) The S order parateter and c) the P order parameter as function of the tube position for each concentration of GO.

orderings, we calculated the average effective birefringence at near edge and the center defined in Eq. (1). Figure 5 exhibits how the average effective birefringence changed as the concentration of GO varies. As shown in Fig. 5, the average effective birefringence at the center was almost linearly increased as the GO concentration increased, and the same trend was observed in the edge at low concentrations. However, the average effective birefringence in the edge was further increased at higher concentrations. Note that the average effective birefringence in the edge is due to the uniaxial alignment of GO particles, which is related to the *S* order parameter. As the GO concentration approaches to biphasic state

or is in biphase, the GO dispersion has self-assembled ordering tendency to some degree. Whereas, the birefringence in the center, which is related to the *P* ordering, is just in proportional to the concentration, which means there is no increase in the P order parameter. In order to clarify this point, we calculated the *S* and *P* order parameters in the next section.

Order Parameter in the Tube Depending on Concentration

The order parameter was deduced from the following relations [15, 16].

$$\Delta n_{z\varphi} \equiv n_z - n_\varphi = \frac{2}{3}\Delta n_{\max} P(\dot{\gamma}) \tag{4}$$

$$\Delta n_{zr} \equiv n_z - n_r = \Delta n_{\max}\left(S(\dot{\gamma}) + \frac{1}{3}P(\dot{\gamma})\right) \equiv \mathrm{N}S'(\dot{\gamma}) \tag{5}$$

Here, Δn_{max} is the maximum birefringence when the order parameter is 1, and the shear rate,

$$\dot{\gamma} = \left|\frac{dV(r)}{dr}\right| = V_{\text{avg}}\frac{m+2}{R}\left(\frac{r}{R}\right)^{m-1} \tag{6}$$

has the relation with the interger *m* and the velocity,

$$V(r) = V_{\text{avg}}\frac{m+2}{m}\left\{1 - \left(\frac{r}{R}\right)^m\right\} \tag{7}$$

m is phenomenological parameter and it determines the shape of flow profile. For example, when $m = 2$, the flow profile is Laminar flow and as it increases above 2, the flow profile evolves to a kind of turbulent flow that has flat flow profile in the center of tube and steep velocity change in the edge. *m* is 2 for very low velocity [17]. The *P* and *S* in Eqs. (4) and (5) can be acquired by the following values from the experimental measurement.

$$R_{\text{eff\_E}} \approx \Delta n_{\max} S'(R)\int_l \mathrm{d}l \tag{8}$$

$$R_{\text{eff\_C}} \approx \frac{2}{3}\Delta n_{\max}\int_l P(r)\mathrm{d}l \tag{9}$$

where $R_{\text{eff\_E}}$ and $R_{\text{eff\_C}}$ are the retardations at the edge and at the center, respectively. In Eq. (9), the *P* order parameter was found from the best fit curves to the experimental transmittance profile. The detail of the calculation method was explained in our previous work [15]. The *S* order parameter indicates the degree of ordering of **a** vector around the r-axis, and the *P* order parameter represents the anisotropic distribution of **a** vector along z-axis and φ-axis, that is, the difference between the degrees of ordering of **a** vector along z-axis and φ-axis. Since the shape of GO particles can be assumed to be a uniaxial disk, the *P* ordering is mainly caused by the particle mode of mode 2 in Fig. 3(c). The calculation results are shown in Fig. 6. As shown in Fig. 6(a), *m* is higher than 2 for all concentration. This

means that the flow velocity profile is more or less flat in the center and decreases steeply near the edge. Figure 6(b) shows the S order parameter profile for various concentrations. The *S* order parameter increases as the concentration increases. On the other hand, the maximum value of the *P* order parameter at the edge rather decreases as the concentration increases, although it increases near the center part. The decrease in the *P* order parameter appears in biphase. The result implies that the intrinsic spontaneous ordering due to inter-particle interaction hinders the biased broad distribution of a vector along φ-axis. That is, GO particles are likely to align more uniaxially rather than biaxially biased ordering as the concentration increases. Such a tendency was not observed in isotropic phase but it becomes clear in biphase. Thus, we can reasonably conclude that the flow-induced ordering in tube flow is influenced by the spontaneous inter-particle interactions, and as a result, the *S* order parameter increases as the concentration increases but the *P* order parameter decreases. This coincides with the average effective birefringence results shown in Fig. 5.

Conclusion

We measured the flow-induced birefringence profile in a tube flow of GO dispersions as the GO concentration increases. We also calculated the profiles of the *S* and *P* order parameters which indicate the uniaxial ordering and the biased biaxial ordering, respectively. It was found that the birefringence increases linearly in isotropic phase, but it increases more in biphase than the linear line extended from the isotropic phase. Similarly, the *S* order parameter increases as the GO concentration increases, but the P order parameter rather decreases in biphase. All these results implies that the spontaneous ordering tendency of GO particles in biphase enhances the uniaxial *S* ordering but suppresses the *P* ordering. Hence, we can conclude that mode 2 is slightly suppressed by the spontaneous nematic ordering as the GO concentration increases and that the GO are likely to align parallel to each other as the GO concentration increases above biphaic transition concentration.

Funding

This research was supported by Basic Science Research Program through the National Research Foundation of Korea (NRF) funded by the Ministry of Education (No. 2012R1A1A1012167 and No. 2013R1A1A2057455).

References

[1] Loh, K. P., Bao, Q., Eda, G., & Chhowalla, M. (2010). *Nature Chem.*, 2, 1015.
[2] Dreyer, D. R., Park, S., Bielawski, C. W., & Ruoff, R. S. (2010). *Chem. Soc. Rev.*, 39, 228.
[3] Xu, Z., & Gao, C. (2011). *Nat. Commun.*, 2, 571.
[4] Dan, B., Behabtu, N., Martinez, A., Evans, J. S., Kosynkin, D. V., Tour, J. M., Pasquali, M. M., & Smalyukh, I. I. (2011). *Soft Matter*, 7, 11154
[5] Xu, Z., & Gao, C. (2011). *Nat. Commun.*, 2, 571.
[6] Kim, J. E. , Han, T. H., Lee, S. H., Kim, J. Y. Ahn, C. W., Yun, J. M., & Kim, S. O. (2011). *Angew. Chem. Int. Edit.*, 50, 3043–3047.
[7] Guo, F., Kim, F., Han, T. H., Shenoy, V. B., Huang, J. R., & Hurt, H. (2011) *ACS Nano*, 5, 8019–8025.
[8] Shen, T., Hong, S. H., & Song, J. K. (2014). *Nat. Mater.*, 13, 394–399.
[9] Yang, X., Guo, C., Ji, L., Li, Y., & Tu, Y. (2013) *Langmuir*, 29, 8103.
[10] Hummers, W. S., & Offema, R. E. (1958). *J. Am. Chem. Soc.*, 80, 1339–1339.
[11] van der Beek, D., & Lekkerkerker, H. N. W., (2004). *Langmuir*, 20, 8582–8586

[12] Mueller, S., Llewellin, E. W., & Mader, H. M. (2010). *P. Roy. Soc. A-Math Phy.*, 466, 1201–1228.
[13] Singh, A. P., & Rey, A. D. (1998) *Rheol. Acta.*, 37, 30–45.
[14] Jefferey, G. B. (1922). *P. Roy. Soc. A-Math Phy.*, 102(715), 161–179.
[15] Shen, T., Hong, S. H., & Song, J. K. (2015). *Liquid Crystals, 42,* 261–269.
[16] Demus, D., Goodby, J. W., Gray, G. W., & Spiess, H.-W. (1998) Eds., *Handbook of Liquid Crystals*, Vol. 1, Chap. 7, Wiley-VCH, Weinheim, Germany.
[17] Cengel, Y. A. (2004) *Cimbala,* Fluid mechanics: Fundamentals and applications, (Chap. 8), McGraw-Hill Education, New York, USA.